Journal of Power Sources 243 (2013) 958–963

Contents lists available at SciVerse ScienceDirect

Journal of Power Sources

journal homepage: www.elsevier.com/locate/jpowsour

Effect of ultra-low Pt loading on mass activity of polymer electrolyte membrane fuel cells

Ákos Kriston [a], Tianyuan Xie [a], David Gamliel [b], Prabhu Ganesan [a], Branko N. Popov [a,*]

[a] University of South-Carolina, Center for Electrochemical Engineering, Dept. of Chemical Engineering, Columbia, SC 29208, USA
[b] University of Massachusetts-Amherst, Dept. of Chemical Engineering, Amherst, MA 01003, USA

HIGHLIGHTS

- Dependence of electrochemical active area, mass and specific activity on Platinum loading is found.
- Non-linear scaling factor is introduced to estimate the real volumetric catalyst density.
- A new Pt-loading corrected Tafel-approximation is proposed.

ARTICLE INFO

Article history:
Received 6 November 2012
Received in revised form
4 May 2013
Accepted 20 May 2013
Available online 29 May 2013

Keywords:
Fuel cell
Mass activity
Pt loading
Electrochemical active surface area (ECSA)

ABSTRACT

The mass activity is intensively used as characterization parameters for evaluation of the effectiveness of the cathode catalyst in polymer electrolyte membrane (PEM) fuel cells. In this work, the dependence of mass activity on platinum loading was studied at the cathode. The results indicated that the mass activity and the utilized electrochemical surface area of the catalyst are not independent of the catalyst loading. The electrochemical specific surface area (ECSA) and the mass activity increase as the loading is decreased. The increase of the ECSA is attributed to the increase of the utilization of the catalyst. The commonly applied Tafel-approximation cannot be used to fit the result because the mass activity is controlled not only by R_Ω and the ORR kinetics, but also the utilization of the catalyst, which in turn depends on catalyst loading, the structure of the catalyst layer, the degree of agglomeration, and screening of the catalyst particles. A detailed and more precise definition of mass activity (MA) is given to elucidate the variation of MA with catalyst loading.

1. Introduction

Platinum is considered to be one of the most active oxygen reduction materials for the four-electron reduction of oxygen to water in acidic environments. However, even on pure Pt, potentials in excess of 300 mV are lost from the thermodynamic potential for oxygen reduction due to competing water activation reaction and sluggish kinetics. If the use of PEMFC in transportation becomes a reality, the large required amount of Pt/C catalyst will cause an enormous increase of Pt demand that will result in a dramatic increase in platinum price. To alleviate this problem, research has been conducted to improve catalyst activity and durability while decreasing the catalyst cost through developing a catalyst with ultra-low platinum loading. The ultimate research goal is to develop a cathode catalyst with platinum group metal content (PGM) lower than 0.2 g PGM kW^{-1} and approach 0.1 g PGM kW^{-1}.

In the recent years, extensive efforts have been undertaken in order to develop different PtM (M = Co, Ni, Fe, Cu) alloys [1] or Pt-skin catalysts [2]. The activities of these catalysts were found to be 2–4 times higher than that of the state-of-the-art Pt/C catalysts. The parameters for catalyst activity, however, have not yet been universally defined.

Gasteiger et al. [3], in their study of the dependence of polymer electrolyte membrane (PEM) fuel cell performance at different Pt catalyst loadings (0.4, 0.24, and 0.15 mg_{Pt} cm^{-2}), have concluded that mass activity (MA) and ECSA (utilization) in cathode catalyst membranes (CCMs) are essentially independent of Pt loading. Saha [4] found that the utilization of a printed CCM layer decreased as the loading of the catalyst layer increased from 0.02 to 0.12 mg cm^{-2}. Lee et al. [5] observed that the mass activity measured in membrane electrode assemblies (MEAs) is only 10–30% of the ring disk electrode (RDE) mass activity, and increased as loading decreased while the utilization was held constant. They concluded that O_2 may access the catalyst particles more effectively when it exhibits thin layer geometry, or higher porosities at lower loadings.

* Corresponding author. Tel.: +1 (803) 777 7314; fax: +1 (803) 777 8265.
E-mail address: popov@engr.sc.edu (B.N. Popov).

0378-7753/$ – see front matter © 2013 Elsevier B.V. All rights reserved.
http://dx.doi.org/10.1016/j.jpowsour.2013.05.078

Debe [6] concluded that the enhanced oxygen reduction reaction (ORR) activity of the Nano Structured Thin Film (NSTF) 3 M catalysts is a result of asymmetrical surface area distribution. The asymmetrical surface area controls the gas velocity distributions in the Knudsen regime, which results in an additional pre-exponential scaling factor in the Butler–Volmer equation dependent on a distance metric describing the catalyst surface area distribution. The catalyst loading influenced the surface enhancement factor (SEF) and consequently the scaling factor.

Siddique et al. [7] developed a catalyst layer microscopic model mimicking the experimental fabrication. The variation of the number of agglomerates varied the ECSA due to reduced connectivity and increased isolation. Large agglomerates correspond to insufficient mixing of ionomer and Pt/C and, consequently, limited triple phase boundaries. Too small of an agglomerate size may lead to the loss of connectivity or entanglement between them.

According to recent studies, the electrode fabrication method has a profound effect on optimal Pt loadings and utilization [8–15] and therefore the measurable mass activity. Numerous studies were performed, but no final agreement has been achieved regarding what mass activity and specific activity characterize, even in flooded agglomerates [16,17], and what experimental conditions are necessary if the catalyst activity is of importance [18,19]. Therefore, in this work we studied both mass activity (MA) and specific activity (SA) in detail for a better understanding of the effects of the catalyst loading on these parameters.

2. Experimental

2.1. Preparation of MEAs of different catalyst loading

The catalyst inks used in the MEAs were prepared by ultrasonically mixing 46% Pt/C catalyst synthesized at USC [20] with water and absolute ethanol. The ionomer in the catalyst ink was maintained at 30 and 20 wt.% for the anode and cathode, respectively. The cathode catalyst ink was sprayed directly on Nafion® 212 membrane and the anode was sprayed on the SGL 10 BC gas diffusion layer (GDL). The Pt loading was periodically measured using X-ray fluorescence spectroscopy (XRF, Fischer XDAC) until the desired catalyst loading was achieved. Finally, the cathode catalyst coated membrane was sandwiched between the catalyst coated gas diffusion layer (GDL) (anode) and bare SGL 10 BC (from SGL Carbon) under a pressure of 25 kg cm^{-2} at 140 °C. The Pt loading was accurately measured using a 5 digit accuracy balance and compared with the results obtained using X-ray fluorescence measurements. The difference in the two measurements of Pt loading was 0.01 mg cm^{-2}, which was taken into consideration for the calculation of absolute error in the mass loading.

2.2. Electrochemical characterization

All the electrochemical characterization studies were performed in 0.1 M $HClO_4$ using a Pine bipotentiostat (Model AFCBP1), a Pt-wire counter electrode, and a saturated Ag/AgCl reference electrode (0.258 V vs. reversible hydrogen electrode (RHE) in 0.1 $HClO_4$ electrolyte). A rotating ring-disk electrode (RRDE) with a Pt ring and glassy carbon disk (surface area of 0.247 cm^2) was used as the working electrode. The catalyst ink was prepared by blending the catalyst powder with ethanol in an ultrasonic bath. Cyclic voltammograms (CVs) recorded in nitrogen were used to obtain the background capacitive currents and ECSA of the Pt catalysts.

The fuel cell performance of the 46% Pt/C catalyst at different Pt loadings was evaluated in a 25 cm^2 single cell under conditions suggested by the U.S. DRIVE Partnership, Fuel Cell Technical Team Cell Component Accelerated Stress Test and Polarization Curve Protocols for Polymer Electrolyte Membrane Fuel Cells. Catalyst MA and polarization studies were performed under H_2/O_2, at 80 °C and 100% relative humidity (RH). Other fuel cell operating conditions are provided in the respective figures. The MA and SA were determined by measuring the current at 0.9 $V_{iR\text{-free}}$.

Prior to the ECSA measurements in the MEA and the RRDE, the Pt catalyst particle surface was cleaned using the following procedures: In the case of MEA, the potential was kept constant at 0.6 V under H_2/O_2 until the current reached a stable value. For the RRDE measurements, the surface cleaning was performed by cycling the potential between 0.3 and 0.8 V (vs. RHE). These surface activation procedures resulted in reliable ECSA measurements and prevented the catalyst agglomeration that occurs during high potential limits.

The ECSA of Pt was determined by charge integration under the hydrogen desorption peaks appearing between 0 and 0.35 V, by assuming a charge of 210 μC cm^{-2} for the electroactive Pt surface. Then, the specific ECSA was calculated based on the following relation [21–25]:

$$A_{Pt,el} = \frac{Q_H}{m \times q_H} \quad (1)$$

where Q_H (μC) is the charge of hydrogen desorption, m (μg cm^{-2}) is the Pt metal loading, and q_H (μC cm^{-2}) is the charge required for desorbing a monolayer of hydrogen on a Pt surface.

The porosity of the catalyst coated membrane (CCM) was measured by a mercury porosimeter (Micromeritics Autopore 9500). The cumulative pore volume as a function of pore diameter was determined from the mercury intrusion data, i.e. the volume of mercury penetrating into the pores versus the applied pressure. Under the assumption that all pores are cylindrical, the pore diameter d_p was calculated from the value of the applied pressure p using the capillary law [26].

$$d_p = \frac{4\gamma\cos\theta}{p} \quad (2)$$

where γ and θ denote the surface tension of mercury and the contact angle between mercury and the sample.

3. Results and discussion

Fig. 1 shows the XRD and TEM image of the Pt/C catalyst. It is shown that the catalyst deposited uniformly on the surface of the carbon support. The particle's average diameter was calculated by using the Debeye–Scherrer equation. The average particle diameter was found to be 2.7 nm.

The thin layer-RDE method revealed that the ECSA is 85 $m^2\ g^{-1}$, which is very close to the theoretically expected value.

Fig. 2 exhibits the hydrogen adsorption and desorption peaks in the cyclic voltammograms recorded for different cathode Pt loading in a 25 cm^2 MEAs. The total charge for the hydrogen adsorption/desorption increased as the Pt catalyst loading increased in the MEAs. As expected, the current in the double layer region also increased with an increase in the Pt loading. The specific electrochemical surface area of Pt was calculated using Equation (1) by integrating the charge under hydrogen desorption peaks appearing between 0.05 and 0.35 V (vs. RHE). The ECSA was calculated by assuming a charge of 210 μC cm^{-2} required for the desorption of a monolayer of H^+ on a smooth Pt planar electrode surface [21]. The ECSA values given in Table 1 show a decrease in the ECSA with an increase in the Pt loading which indicates that $A_{Pt,el}$ (ECSA) depends on the Pt loading. The increase in the ECSA at lower catalyst loading (0.05 $mg_{Pt}\ cm^{-2}$) may be attributed to the fact that the Pt catalyst particles are uniformly distributed at a thin catalyst layer on the

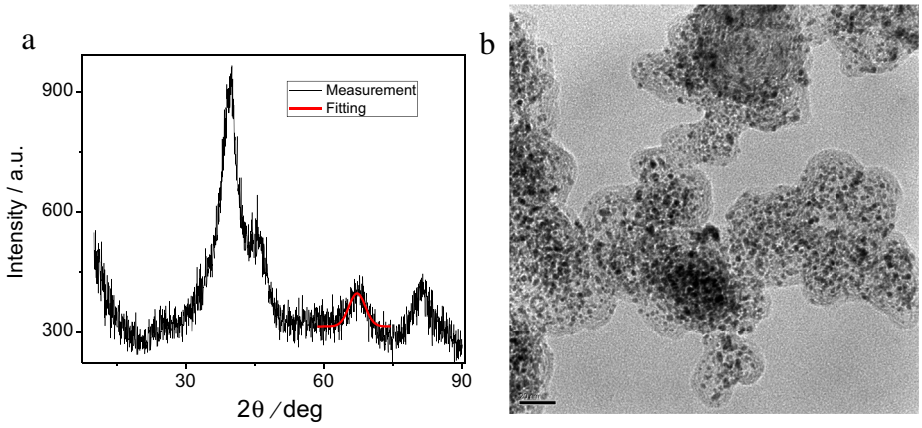

Fig. 1. XRD spectrum of the 46% Pt/C catalyst. Average particle size is 2.7 nm (a) and the HR-TEM image at 20 nm resolution (b).

Nafion® membrane with minimum particle agglomeration. This increases the availability of Pt catalyst active sites for oxygen reduction resulting in maximum catalyst utilization. Table 1 also demonstrates that the catalyst utilization for different MEAs decreased from 82% to 48% when the Pt loading is increased from 0.05 to 0.4 mg_{Pt} cm^{-2}. The utilization of the Pt catalyst depends on how effectively the catalyst particles are connected to: (i) the ionic conductor Nafion® membrane and (ii) the electronic conductor gas diffusion layer (GDL). If the thickness of the catalyst layer increases, the probability of the percolation of the reactants through the catalyst layer may decrease. Hence, the reactants may not reach the Pt catalytic sites that are far away from the Nafion® membrane/GDL interface resulting in lower catalyst utilization at higher catalyst loadings.

Fig. 3 presents the effect of 46% Pt/C loading on the current density. The fuel cell was operated at 80 °C under H_2/O_2 (750/750 ml min^{-1}), 100% RH and ambient pressure to measure the initial performance of MEAs with different Pt loadings under H_2/O_2. The catalyst mass activity was determined using the experimental conditions suggested by the U.S. DRIVE Partnership, Fuel Cell Technical Team Cell Component Accelerated Stress Test and Polarization Curve Protocols for Polymer Electrolyte Membrane Fuel Cells. The fuel cell testing conditions are: 80 °C under H_2/O_2 (2/9.5 stoic.), 100% RH and 150 $kPa_{abs.}$ The operating conditions are also given in the figures. The fuel cell performance was evaluated using MEAs prepared with Pt loadings of 0.05, 0.1, 0.2, 0.3 and 0.4 mg cm^{-2}, respectively. Both the high and low current increases as the loading increases, but the increase is more substantial when the loading increases from 0.05 to 0.2 mg cm^{-2}. As expected, the current density measured at 0.9 V (iR-corrected) decreases from 0.035 A cm^{-2} to 0.012 A cm^{-2} measured for Pt loadings between 0.4 mg cm^{-2} and 0.05 mg cm^{-2}.

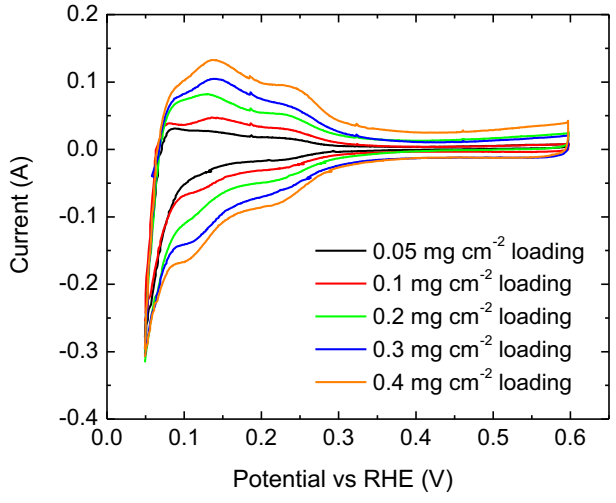

Fig. 2. The CV measurements in MEA at different loadings. Anode: 100% H_2 200 ccm, cathode: 100% N_2 75 ccm, cell temperature 80 °C, 100% RH.

Mass activity is defined as the normalized current density measured at 0.9 V (iR-corrected) divided by the cathode PGM loading in A mg_{PGM}^{-1}. The MA, catalyst loading (L), specific activity (SA), specific electrochemical surface area (ECSA), or surface enhancement factor (SEF) can be calculated if three of the five parameters are known by using the following equations:

$$MA = \frac{i_{0.9\ V}}{L} \tag{3}$$

$$SA = \frac{i_{0.9\ V}}{L \cdot ECSA_{MEA}} \tag{4}$$

$$SEF_{MEA} = ECSA_{MEA} \cdot L \tag{5}$$

where $i_{0.9\ V}$ is the current density measured at 0.9 $V_{iR\text{-}free}$ and normalized to the geometrical surface area (A cm^{-2}), here L is specifically the Pt loading (mg cm^{-2}), SEF_{MEA} is the surface enhancement factor (cm^2_{Pt} cm^{-2}), SA is the specific activity (A cm^{-2}_{Pt}) and MA is the mass activity (A mg^{-1}_{Pt}).

MA is evaluated by Tafel-equation. This equation is valid under the assumption that the surface area of the individual particles can be linearly added and is linearly proportional to the mass of the catalyst.

Table 1
Comparison of electrochemical properties for different Pt loadings.

Pt loading (mg cm^{-2})	Current density @ 0.9 $V_{iR\text{-}free}$ (A cm^{-2})	ECSA fuel cell/RDE (m^2 g^{-1})	Utilization (%)
0.05	0.012	70/85	82
0.1	0.0185	68/85	80
0.2	0.03	64/85	75
0.3	0.0321	48/85	56
0.4	0.035	41/85	48

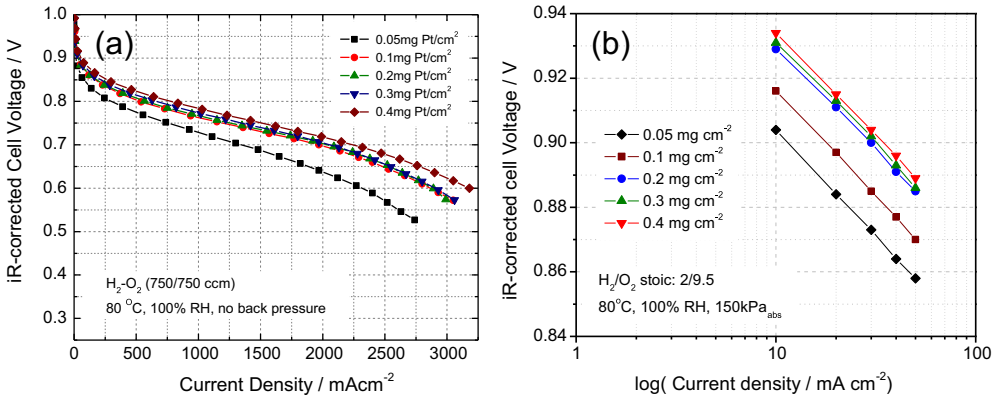

Fig. 3. Effects of Pt loading on the H_2–O_2 fuel cell performance at high (a) and low current (b).

$$\eta = \mathrm{TS}\log\left(j_{\mathrm{cell}} + j_{\mathrm{H_2}}\right) - \mathrm{TS}[\mathrm{ECSA}\cdot m_{\mathrm{Pt}} j_0] \tag{6}$$

where TS is the Tafel slope, j_{cell} is the measured total cell current density (A cm^{-2}), $j_{\mathrm{H_2}}$ is the hydrogen crossover current density. m_{Pt} is the Pt cathode loading ($\mathrm{mg_{Pt}\ cm^{-2}}$). It has been reported in the literature that $j_{\mathrm{cell}} = j + j_x$, where j_x is the measured hydrogen crossover current with a value of 3.3 mA cm^{-2} [3]. The hydrogen crossover current can vary depending on the experimental conditions.

Eq. (6) requires the polarization of the CCMs with different Pt loadings. When plotted, the following should yield identical slopes: $E_{\mathrm{iR\text{-}free}}$ vs. the log $(j_{\mathrm{cell}} + j_{\mathrm{H_2}}/m_{\mathrm{Pt}})$ and $E_{\mathrm{iR\text{-}free}}$ vs. log of mass activity A $\mathrm{mg_{Pt}^{-1}}$ (the mass specific current density, j_{m}). With this assumption, the cathode performance is controlled only by the ORR kinetics and the Ohmic losses (R_Ω), or:

$$\left[\frac{\Delta E_{\mathrm{iR-free}}}{\Delta \log\left[i_{\mathrm{m}}\right]}\right]_{P_{O_2'}P_{H_2},\ T,\ A_{\mathrm{Pt,el}}} = -\mathrm{TS} \tag{7}$$

Fig. 4 shows the MA and SA at different loadings. An increase of MA up to 0.23 A $\mathrm{mg_{Pt}^{-1}}$ was observed for 0.05 $\mathrm{mg_{metal}\ cm^{-2}}$ loadings, compared with a MA of 0.085 A $\mathrm{mg_{Pt}^{-1}}$ measured for Pt loadings of 0.4 mg cm^{-2}. However, as shown in Table 2 and the prediction of Eq. (6), the MA increases when the loading decreases, which may be related to the increase in ECSA from 41 to 70 $\mathrm{m^2\ g^{-1}}$. The ECSA increase is a consequence of the catalyst utilization (Table 1) calculated from the ECSA of the thin-layer film RDE. The effect of the ECSA can be evaluated by substituting the current density for the specific current. The result shows (Table 2) that the SA increased from 213 μA $\mathrm{cm_{Pt}^{-2}}$ to 343 $\mu\mathrm{A}^{-2}\mathrm{cm_{Pt}^{-2}}$ when the loading decreased from 0.4 mg cm^{-2} to 0.05 mg cm^{-2}. The MA and SA increased by a factor of 2.7 and 1.6, respectively while the ECSA increased to 1.7 times from its original value. This implies that the ECSA only partially accounted for the increase in MA. Consequently, the structure of the active layer or the reaction path may have also changed. Inaba et al. [27] showed that the increase of Pt loading altered the agglomeration of the Pt/C catalyst on RDE disk. Bonakdarpour [28] varied the loadings on nano structured thin film catalysts (3 M), and found that the reaction mechanism of the ORR changed. The lower loadings or increased catalyst agglomeration altered the reaction path of the ORR, which was attributed to the sparsely distributed active sites. The slopes of the log i_{Pt}–V and log i_{m}–V plots were almost identical to the theoretically expected values for the different Pt loadings, which indicate that the MEAs were kinetically controlled and the reaction path did not change. Consequently, the increased MA points out that the MA curves cannot be reasonably predicted by Eq. (6), therefore the polarization curves obtained in this study for 46% Pt/C catalyst cannot be fitted with Eq.(6).

According to the experimental results, the MA is controlled not only by R_Ω and the ORR kinetics, but also by the utilization of the Pt surface area which in turn depends on the cathode Pt loading shown in Table 1. The MA is also controlled by the morphology of the catalyst layer which depends on the self-assembled nature of the catalyst and how effectively it fills out the volume.

Table 3 shows the specific surface area, the average pore size, and the porosity of the catalyst layer at different loadings. The data clearly shows that the loading highly influenced the physical properties of the catalyst layer. The specific surface area decreased from 754 to 212 $\mathrm{m^2\ g^{-1}}$ as the loading increased from 0.05 to

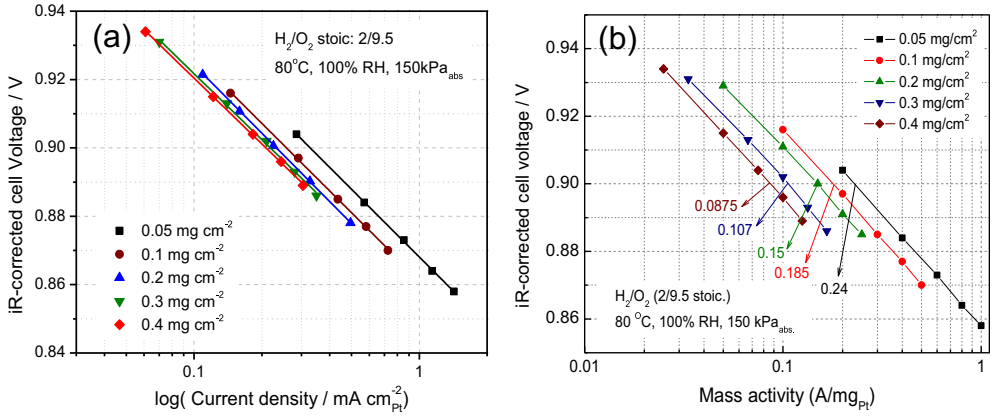

Fig. 4. Effect of Pt loading on the (a) specific and (b) mass activity of MEAs under DOE fuel cell operating conditions.

Table 2
Summary of the measured values and calculated mass and specific activities of the H_2–O_2 fuel cells performance.

Pt loading (mg cm^{-2})	Tafel slope (V/dec)	Specific activity (μA cm$_{Pt}^{-2}$)	Mass activity (mA mg^{-1})
0.05	−0.065	343	240
0.1	−0.065	272	185
0.2	−0.063	234	150
0.3	−0.064	223	107
0.4	−0.063	213	87.5

0.4 mg cm^{-2}. This suggests that the newly deposited particles stick to the previous ones and screen each other's surfaces.

The variation of the pore diameter is shown in Fig. 5. At 0.05 mg cm^{-2} loadings the pore size between the agglomerates is about 12 nm, but at higher loadings (0.4 mg cm^{-2}) it shifts to around 40 nm. Simultaneously, the pores smaller than 20 nm diminish. The porosity was almost the same between 39% and 42% at 0.05 and 0.4 mg cm^{-1} loadings, respectively. At 0.05 mg cm^{-2} the porosity shows a higher value (39%) than 0.1 mg cm^{-2} (31%), probably because the particles first coat the membrane and after 100% coverage they start to overlap with the previous layers. Above 0.1 mg cm^{-2} a clear increasing trend is shown from 31% to 43% as the loading increases from 0.1 mg cm^{-2} to 0.4 mg cm^{-2}.

The results can be explained by taking into account that in PEM fuel cells, the catalyst forms triple phase boundaries (TPB) in a 3D structure of gas, catalyst, and electrolyte, which makes the experiments and the evaluation of the data more complex than for simply flooded agglomerates [16]. Agglomerate and macro-homogeneous models have been developed to model the polarization curve. However, they have no general solution although different asymptotic solutions have been derived. One of the first solutions was developed by Perry and Newman et al. [29]. When both diffusion and proton migration are not limiting (as in the kinetic region), the following expression can be derived:

$$i = -i_0 a_{Pt} \frac{c}{c_0} l_{CL} \exp\left(-\frac{RT}{\alpha F}\cdot\eta^c\right) \quad (8)$$

where a_{Pt} (cm^2 cm^{-3}) is the area of the active catalyst per unit volume, i_0 (A cm^{-2}) is the exchange current density, and l_{CL} (cm) is the catalyst layer thickness (theoretical value), α is the symmetry factor of the charge transfer, c (mol cm^{-3}) is the oxygen concentration at the catalyst interface, and c_o (mol cm^{-3}) is the reference concentration. This model, however, does not take the Pt loading into consideration.

Jaouen [30] et al. developed a spherical agglomerate model and also determined the asymptotic solutions. In the kinetic region it was found that:

$$i = -a_{Pt} i_0 l_{CL} \frac{c}{c_0}(1-\varepsilon_1)(1-\varepsilon_2)\exp\left(-\frac{RT}{\alpha F}\cdot\eta^c\right) \quad (9)$$

where ε_1 is the polymer volume fraction inside the agglomerate, and ε_2 is the gas-phase porosity (macroporosity), T is the temperature (K) and R is the universal gas constant. In his model the current depends on the structure of the active layer. The general

Table 3
Physical characterization of the pore structure of the CL at different Pt loadings.

Loading	Specific surface area/m^2 g^{-1}	Pore diameter (μm)	Porosity (%)
0.05	754	0.012	39
0.1	557	0.011	31
0.3	244	0.044	34
0.4	212	0.0391	43

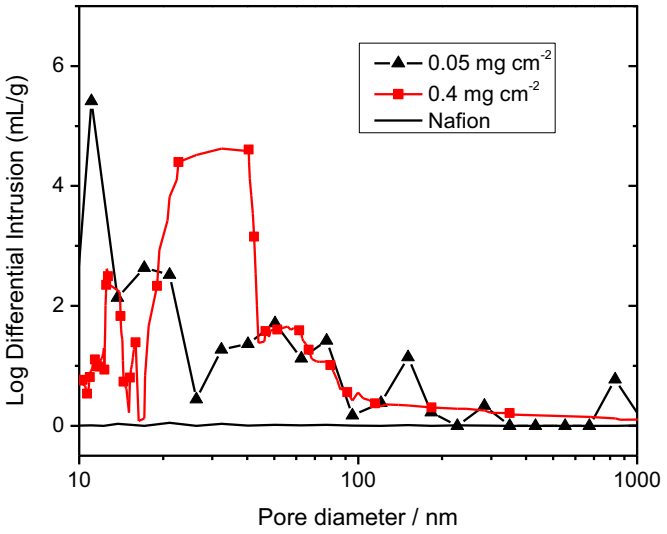

Fig. 5. Differential pore volume at 0.05 (▲) and 0.4 mg cm^{-2} (■) Pt loadings CCM and the catalyst free Nafion (line).

theory of dimensionless analysis and asymptotic solutions were developed by Gyenge [31], but in the kinetic region he derived the same relationship as Eqs. (6)–(7).

The Pt active area per unit volume is commonly determined by Ref. [32–35]

$$a_{Pt} = \frac{m_{Pt}\nu_{Pt}ECSA_{RDE}}{W_{CL}} \quad (10)$$

where $ECSA_{RDE}$ is the specific ECSA of the catalyst (m^2 g^{-1}), measured using thin-layer RDE and ν_{Pt} is the catalyst utilization. The thickness, W_{CL} (cm), can be calculated by assuming the conservation of volume. This model indicates that the ECSA and the structure are independent on the loading, and consequently leads to the same linear scaling approach between loading and the volumetric specific surface area as the Tafel-approximation, i.e. a_{Pt} is independent on the loading. Contrarily, Gu et al. [36] concluded that Pt and C act as the structural element, while the ionomer essentially fills out the voids. Pt particles smaller than 1.7 nm are mainly incorporated into the pores while bigger particles (3–5 nm) are mainly found on the surface [37]. Zhang et al. [38] also concluded that Pt particles are in the mesopores and Nafion® primarily presents on the external surface, blocking the micropores but not the macropores. Gode et al. studied the effects of Nafion® loading by using different porosimetry and simulation techniques [39]. First, they observed that the increase in Nafion® ratio did not increase the layer thickness linearly. Second, Nafion® first covered the micropores (<2 nm) and later the meso- and macropores. This result indicates that the volume and the thickness depend on how the catalyst layer is formed, how the particles connect to each other and how they fill out the volume. Therefore Eq. (10) should be precisely calculated as the quotient of the total surface area of the catalyst (A_{tot}) and the total volume of the catalyst layer (V_{tot}).

$$a_{Pt} = \frac{A_{tot}}{V_{tot}} = \frac{ECSA\cdot M_{Pt}}{V_{tot}} = ECSA(M_{Pt})\rho_{Pt}(M_{Pt}) \quad (11)$$

where M_{Pt} (mg) is the total Pt loading and $\rho_{Pt}(M_{Pt})$ (mg cm^{-3}) is the loading dependent Pt density in the agglomerates or in the CL. Eq. (10) is valid only if the ECSA and the ρ_{Pt} are to be independent of the loading. However, the measured data shown in Table 1 indicate that the ECSA depends on the loading. The catalyst density may also

dependon the loading which were summarized previously according to Refs. [36–39]. Introducing a non-linear scaling factor, similar to the utilization of the ECSA (Table 1), Eq. (11) can be rewritten into the following form

$$a_{Pt} = ECSA \cdot \nu_{MEA} \rho_{Pt} P_{MEA} \quad (12)$$

where ν_{MEA} is the catalyst utilization (%) of the MEA at different loadings and P_{MEA} is the non-linear scaling factor (%). While ρ_{Pt} now does not depend on the loading, it can be calculated by dividing it with the geometrical surface area:

$$\rho_{Pt} = \frac{M_{Pt}}{V_{CL}} = \frac{m_{Pt}}{W_{CL}} \quad (13)$$

and Eq. (10) becomes

$$a_{Pt} = ECSA \cdot \nu_{MEA} \frac{m_{Pt}}{W_{CL}} P_{MEA} \quad (14)$$

The W_{CL} is the average thickness predicted by the spherical agglomerate model. The real thickness of the catalyst layer is very difficult to determine by STEM measurement, because the surface of the CL is very rough (non-uniform).

The combination of the asymptotic solutions of the macro homogeneous and agglomerate models Eqs. (8) and (9) and the new form of the surface area per unit volume of the cathode CL Eq. (14) renders the log i–V relationship with the following general form:

$$\eta_0 = TS \ln \left[\frac{j_{cell}}{ECSA \cdot \nu_{MEA} i_0 P_{MEA} m_{Pt}} \left(\frac{c^{O_2}_{REF}}{c^{O_2}_{GDL}} \right)^{\gamma} \right] \quad (15)$$

Substituting $(j_{cell}/m_{Pt}) = i_m$ with the mass specific current and using the log identities we reach

$$\eta = TS\ln(i_m) - TS\ln \left(ECSA \cdot \nu_{MEA} i_0 P_{MEA} \left(\frac{c^{O_2}_{GDL}}{c^{O_2}_{REF}} \right)^{\gamma} \right) \quad (16)$$

Also including $(j_{cell}/ECSA \cdot \nu_{MEA} m_{Pt}) = i_{Pt}$ we reach

$$\eta = TS\ln(i_{Pt}) - TS\ln \left(i_0 P_{MEA} \left(\frac{c^{O_2}_{GDL}}{c^{O_2}_{REF}} \right)^{\gamma} \right) \quad (17)$$

which are both Tafel-type equations, however the constants are different from the original Tafel equation. It is evident that the non-linear scaling factor influences both the MA and SA.

4. Conclusion

Our experimental data showed that the electrochemical specific surface area (ECSA), MA, and SA all increase as the loading decreases. The increase of the ECSA is attributed to the increase of the utilization of the catalyst as they are closer to the membrane and to the GDL in a thinner layer. The increase of the ECSA indicates that the commonly applied Tafel-approximation cannot be fitted to our result because the MA and SA are controlled not only by R_Ω and the ORR kinetics but also by the utilization of the catalyst, which in turn depends on catalyst loading, the structure of the catalyst layer, the degree of agglomeration, and screening of the catalyst particles.

A detailed and more precise definition of mass activity (MA) and specific activity (SA) was given to elucidate the variation of MA and SA with catalyst loading. The asymptotic solution of the agglomerate macro homogeneous model has been applied in order to elucidate the dependence of MA and SA on catalyst loading. In the spherical agglomerate model, the surface area per unit volume is regarded as independent of the loading. However, as in the case of the ECSA, it may also depend on the loading and the thickness of the CL. A new non-linear scaling factor has been introduced which considers the effect of the loading on the volumetric agglomerate density. Finally, the loading dependent Tafel equation has been derived. This model contains both the utilization and the non-linear scaling factor. First principle model will be developed in our future work which will explain quantitatively the dependence of mass activity on the loading.

Acknowledgement

The financial support of National Science Foundation (0966956) and Department of Energy (DE-EE0000460) are acknowledged gratefully.

References

[1] K.C. Neyerlin, R. Srivastava, C. Yu, P. Strasser, J. Power Sources 186 (2009) 261–267.
[2] V.R. Stamenkovic, B. Fowler, B.S. Mun, G. Wang, P.N. Ross, C.A. Lucas, N.M. Marković, Science 315 (2007) 493–497.
[3] H.A. Gasteiger, J.E. Panels, S.G. Yan, J. Power Sources 127 (2004) 162–171.
[4] M.S. Saha, D. Malevich, E. Halliop, J.G. Pharoah, B.A. Peppley, K. Karan, J. Electrochem. Soc. 158 (2011) B562–B567.
[5] M. Lee, M.A. Donald, T.H. Uchida, M. Watanabe, Electrochim. Acta 56 (2011) 4783–4790.
[6] Mark K. Debe, J. Electrochem. Soc. 159 (2012) B54–B67.
[7] N.A. Siddique, F. Liu, Electrochim. Acta 55 (2010) 5357–5366.
[8] H.A. Gasteiger, S.S. Kocha, B. Sompalli, F.T. Wagner, Appl. Catal. B: Environ. 56 (2005) 9–35.
[9] F. Jaouen, F. Charreteur, J.P. Dodelet, J. Electrochem. Soc. 153 (2006) A689–A698.
[10] M. Yuasa, A. Yamaguchi, H. Itsuki, K. Tanaka, M. Yamamoto, K. Oyaizu, Chem. Mater. 17 (2005) 4278.
[11] K. Suzuki, N. Sawai, J. Electrochem. Soc. 151 (2004) A2132–A2137.
[12] D. Villers, X. Jacques-Bedard, J.P. Dodelet, J. Electrochem. Soc. 151 (2004) A1507–A1515.
[13] P. Mani, R. Srivastava, P. Strasser, J. Phys. Chem. C 112 (2008) 2770–2778.
[14] P. Mani, R. Srivastava, P. Strasser, J. Power Sources 196 (2011) 666–673.
[15] F.T. Wagner, B. Lakshmanan, M.F. Mathias, J. Phys. Chem. Lett. 1 (2010) 2204–2219.
[16] K. Kinsohita, Electrochemical Oxygen Technologies, John Wiley & Sons, New York, 1992.
[17] M. Watanabe, H. Sei, P. Stonehart, J. Electroanal. Chem. Interfacial Electrochem. 261 (1989) 375–387.
[18] M. Nesselberger, S. Ashton, J.C. Meier, I. Katsounaros, K.J.J. Mayrhofer, M. Arenz, J. Am. Chem. Soc. 133 (2011) 17428–17433.
[19] I.E.L. Stephens, A.S. Bondarenko, U. Grønbjerg, J. Rossmeisl, I. Chorkendorff, Energy Environ. Sci. 5 (2012) 6744–6762.
[20] B.N. Popov, X. Li, G. Liu, J.W. Lee, Int. J. Hydrogen Energy 36 (2011) 1794–1802.
[21] H. Angerstein-Kozlowska, in: E. Yeager, J.O.M. Bockris, B.E. Conway, S. Sarangapani (Eds.), Comprehensive Treatise of Electrochemistry vol. 9, PlenumPress, New York, 1984. (Chapter 2).
[22] S. Huang, P. Ganesan, B.N. Popov, ACS Catal. 2 (2012) 825–831.
[23] S. Huang, P. Ganesan, B.N. Popov, Appl. Catal. B: Environ. 102 (2011) 71–77.
[24] S. Huang, P. Ganesan, B.N. Popov, Appl. Catal. B: Environ. 96 (2010) 224–231.
[25] S. Huang, P. Ganesan, S. Park, B.N. Popov, J. Am. Chem. Soc. 131 (2009) 13898–13899.
[26] A.J. Bard, L.R. Faulkner, Electrochemical Methods, second ed., John Wiley & Sons, New York, 2001, pp. 156–226.
[27] M. Inaba, H. Yamada, J. Tokunaga, A. Tasaka, Electrochem. Solid-State Lett. 7 (2004) A474–A476.
[28] A. Bonakdarpour, T.R. Dahn, R.T. Atanasoski, M.K. Debe, Electrochem. Solid-State Lett. 11 (2008) B208–B211.
[29] M. Perry, J. Newman, E.J. Cairns, J. Electrochem. Soc. 145 (1998) 5–15.
[30] F. Jaouen, G. Lindbergh, G. Sundholm, J. Electrochem. Soc. 149 (2002) A437–A447.
[31] E.L. Gyenge, J. Power Sources 152 (2005) 105–121.
[32] Á. Kriston, G. Inzelt, I. Faragó, T. Szabó, Comp. Chem. Eng. 34 (2010) 339–348.
[33] W. Suna, B.A. Peppley, K. Karan, Electrochim. Acta 50 (2005) 3359–3374.
[34] A. Weber, W. Yoon, J. Electrochem. Soc. 158 (2011) B1007–B1018.
[35] S. Litster, N. Djilali, Electrochim. Acta 52 (2007) 3849–3862.
[36] H. Yokokawa, H.A. Gasteiger, W. Vielstich (Eds.), Handbook of Fuel Cells – Fundamentals, Technology and Applications, John Wiley & Sons, New York, 2009, p. 10.
[37] G. Lin, D. Hong-da, L. Bao-hua, K. Fei-yu, New Carbon Mater. 25 (2010) 53–59.
[38] J.Z. Zhang, K. Hongsirikarn, J.G. Goodwin Jr., J. Power Sources 196 (2011) 7957–7966.
[39] P. Gode, F. Jaouen, G. Lindbergh, A. Lundblad, G. Sundholm, Electrochim. Acta 48 (2003) 4175–4187.